12536–12550 *Nucleic Acids Research, 2017, Vol. 45, No. 21* *Published online 13 October 2017*
doi: 10.1093/nar/gkx886

Molecular basis for asymmetry sensing of siRNAs by the *Drosophila* Loqs-PD/Dcr-2 complex in RNA interference

Jan-Niklas Tants[1,2,†], Stephanie Fesser[3,†], Thomas Kern[1,2], Ralf Stehle[1,2], Arie Geerlof[1], Christoph Wunderlich[4], Michael Juen[4], Christoph Hartlmüller[1,2], Romy Böttcher[3], Stefan Kunzelmann[3], Oliver Lange[2], Christoph Kreutz[4], Klaus Förstemann[3,*] and Michael Sattler[1,2,*]

[1]Institute of Structural Biology, Helmholtz Zentrum München, 85764 Neuherberg, Germany, [2]Center for Integrated Protein Science Munich at Chair of Biomolecular NMR Spectroscopy, Department Chemie, Technische Universität München, 85748 Garching, Germany, [3]Genzentrum & Department Biochemie, Ludwig-Maximilians-Universität, 81377 München, Germany and [4]Institute of Organic Chemistry and Center for Molecular Biosciences CMBI, Universität Innsbruck, 6020 Innsbruck, Austria

Received April 03, 2017; Revised September 22, 2017; Editorial Decision September 22, 2017; Accepted September 22, 2017

ABSTRACT

RNA interference defends against RNA viruses and retro-elements within an organism's genome. It is triggered by duplex siRNAs, of which one strand is selected to confer sequence-specificity to the RNA induced silencing complex (RISC). In *Drosophila*, Dicer-2 (Dcr-2) and the double-stranded RNA binding domain (dsRBD) protein R2D2 form the RISC loading complex (RLC) and select one strand of exogenous siRNAs according to the relative thermodynamic stability of base-pairing at either end. Through genome editing we demonstrate that Loqs-PD, the *Drosophila* homolog of human TAR RNA binding protein (TRBP) and a paralog of R2D2, forms an alternative RLC with Dcr-2 that is required for strand choice of endogenous siRNAs in S2 cells. Two canonical dsRBDs in Loqs-PD bind to siRNAs with enhanced affinity compared to miRNA/miRNA* duplexes. Structural analysis, NMR and biophysical experiments indicate that the Loqs-PD dsRBDs can slide along the RNA duplex to the ends of the siRNA. A moderate but notable binding preference for the thermodynamically more stable siRNA end by Loqs-PD alone is greatly amplified in complex with Dcr-2 to initiate strand discrimination by asymmetry sensing in the RLC.

INTRODUCTION

RNA interference (RNAi) is a sequence-specific RNA degradation process that serves to defend against invading RNA viruses (1–3) and retro-transposons (4–7). RNAi is triggered by double-stranded RNA (dsRNA), which is processed into 21 nt siRNA duplexes with 2 nt 3′-overhangs by the RNase III family enzyme Dicer. In *Drosophila melanogaster*, Dcr-2 is dedicated to the processing of dsRNA into siRNAs, whereas Dcr-1 operates in the related microRNA (miRNA) pathway. A common theme in the biogenesis of both miRNAs and siRNAs is the pairing of an RNaseIII-family nuclease with a small partner protein that contains two or more instances of the dsRNA binding domain (dsRBD) (8–14). While virus-derived sequences are called siRNAs, the transposon-targeting sequences are usually referred to as endo-siRNAs to point out their endogenous origin.

The dsRBD has a conserved fold with αββα topology (15,16) that mediates binding to double-stranded RNA molecules as well as protein–protein interactions (17). Structural studies of RNA-bound domains revealed mainly contacts to the ribose-phosphate backbone of an A-form RNA helix without sequence-specificity (18–20). In certain cases, particular deviations from a perfect dsRNA helix can be specifically recognized by a dsRBD (21). Despite the fact that dsRBDs often occur in multiple instances within the same protein or within a protein complex, only few studies have examined their interplay at the structural level (20–24) or analyzed the roles of tandem dsRBD for RNA binding (18,22,25,26). It is thus important to characterize the molec-

*To whom correspondence should be addressed. Tel: +49 89 289 52600; Fax: +49 89 289 52669; Email: sattler@helmholtz-muenchen.de
Correspondence may also be addressed to Klaus Förstemann. Email: foerstemann@lmb.uni-muenchen.de
†These authors contributed equally to this work as first authors.

ular function and biological activity of tandem dsRBD domains using structural and biophysical approaches combined with functional analysis.

Although the structure of an siRNA duplex is pseudo-symmetric, one strand is preferentially incorporated into RISC. Strand preference depends on the relative stability of base-pairing at either end of the siRNA (referred to as thermodynamic asymmetry sensing), such that the less stably base-paired 5′-end preferentially enters the Argonaute protein. Several mechanisms for strand selection can operate, such as 5′-nucleotide preference (e.g. 5′-U) of the Ago-protein sensing of unpaired nucleotides or phosphorylation state (for synthetic siRNAs) or the formation of specific protein complexes that aid during Ago-loading (27–31). In *Drosophila*, loading of Ago2 with siRNAs depends on the RISC loading complex (RLC) composed of Dcr-2 and the dsRBD protein R2D2 (32–35). The RLC but not Dcr-2 alone binds asymmetrically to duplex siRNAs. Therefore, it has been proposed that R2D2 serves as the sensor for asymmetry detection (32). In humans, it appears that the TRBP/Dicer complex can bind siRNAs asymmetrically (36,37) but this may not be required during small RNA loading (34,38,39). Biochemical studies have demonstrated partial redundancy between the paralogs Loqs-PD and R2D2 (40,41) and deep sequencing experiments have revealed that some Ago2-loaded siRNAs are present even in *r2d2* null mutant animals (42). However, the specific function of Loqs-PD during RISC loading has not been clarified.

Here, we have performed deep sequencing of small RNAs after genome editing in cultured S2-cells to demonstrate that R2D2 can be replaced by its paralog Loqs-PD for loading of endogenous and exogenous siRNAs but not for loading of Ago2-tropic miRNAs. NMR-derived solution structures show that the Loqs dsRBD domains adopt canonical dsRBD folds. Single and tandem dsRBDs can bind independently to RNA with moderate preference for siRNA over pre-miRNA or miRNA/miRNA* substrates. Site-specific cross-linking is most efficient at the siRNA ends and demonstrates that the complex of Dcr-2 with Loqs-PD possesses strand discrimination activity analogous to Dcr-2/R2D2. Notably, NMR data indicate that the dsRBDs slide along the double-stranded RNA helix and do not mediate sequence-specific contacts to the RNA. The tandem dsRBDs of Loqs have a weak but notable preference to bind the more stably base-paired end of an siRNA duplex. This moderate preference is strongly enhanced in the Dcr-2/Loqs-PD complex, indicating their cooperation during the strand selection process. Identification of Loqs-PD as the alternative RISC loading complex subunit has thus allowed us to examine the role of both individual *Drosophila* RLC components during the initiation of guide strand selection. Our results indicate that the dsRBD protein serves as siRNA asymmetry sensor for the alternative RLC, and demonstrate that the combined action of Dcr-2 with Loqs-PD is essential for faithful strand discrimination.

MATERIALS AND METHODS

Protein expression, purification

For expression of full length Loqs-PD (residues 1–359), truncated Loqs-PD$_{\Delta N}$ (residues 129–359), Loqs-PD$_{\Delta NC}$ (residues 129–322) and the two dsRNA-binding domains dsRBD1 (residues 129–211) and dsRBD2 (residues 245–322) a modified pET-M11 vector with an N-terminal His$_6$-ZZ-tag and a following tobacco etch virus (TEV) protease cleavage site was used. All plasmids were verified by sequencing, transformed into *Escherichia coli* BL21 (DE3) cells for protein expression and cultivated in LB or minimal M9T medium containing either or both of 2g/l [U-^{13}C]-glucose and 1g/l ^{15}N ammonium chloride. See supplementary methods for details on the purification procedure. His$_6$-tagged Dcr-2 was expressed in Sf21 cells using the BAC-to-BAC Baculovirus Expression System (Invitrogen), purified via a HisTrap HP column (GE Healthcare) (8) followed by a HiPrep 16/60 Sephacryl S200 gel filtration column (GE Healthcare).

NMR spectroscopy

Proteins and protein–RNA complexes were studied in sodium phosphate buffer pH 6.5 and 7.2. 5% D_2O was added for locking. Protein samples were measured at 298 K and imino NOESY spectra of RNA were recorded at 278 or 298 K. Spectra were recorded on Bruker AVIII 500, AVIII 600, AVIII 750, AVIII 800 and AVIII 900 NMR spectrometers with cryogenic (TCI) triple resonance gradient probes, or standard TXI probes for AVIII 750. Data were processed using Topspin 3.0 and NMRPipe/Draw (43) and analyzed with Sparky 3 (T.D. Goddard and D.G. Kneller, SPARKY 3, University of California, San Francisco, USA). Backbone assignments were derived from HNCA, HNCACB, HNCACO, HNCO and HNCOCACB experiments, side chain assignments were obtained from HCCH-TOCSY, ^{15}N- and ^{13}C-edited NOESY-HSQC experiments (44). NMR titration experiments were performed with individual dsRBD1 or dsRBD2 domains and 21-nt endo-siRNA with 2 nt 3′ overhangs (*ban*-siRNA), (5′-UCAGCUUUCAAAAUGAUCUCACU-3′, 5′-UGAGAUCAUUUUGAAAGCUGAUU-3′) at protein concentrations of 100 μM with protein:RNA ratios as follows: 1:0, 1:0.25, 1:0.5, 1:0.75, 1:1, 1:1.25. For Loqs-PD$_{\Delta NC}$ protein concentrations of 200 μM and molar ratios of 1:0, 1:0.12, 1:0.47, 1:0.7, 1:0.9, 1:1.1 were used. See Supplementary Information for further details.

Binding assays

Please refer to the Supplementary Information for details on RNA sample preparation. 10 nM FITC-labeled RNA oligos were incubated in binding buffer (10 mM Hepes, pH 7.4, 100 mM KAc, 2 mM MgAc and 5 mM DTT) with increasing amounts of recombinant protein for 30 min at RT in a black, non-binding 96-well plate (Greiner bio-one). Anisotropy values were recorded in an Infinite M1000 plate reader (Tecan). For EMSA experiments, binding reactions were mixed 4:1 with binding buffer supplemented with 50% glycerol and resolved on native 4% PAA gels for

20–24 min at 200V. A Typhoon 9400 variable mode imager (GE Healthcare) was used to image the fluorescence signal. Quantification of EMSA bands was performed with Multigauge V3.0 software (FujiFilm), and binding curves were fitted with the Hill equation in Origin 8.1.

Crosslinking experiments

The substrate oligonucleotides were radioactively labeled using polynucleotide kinase (Fermentas) and γ^{32}P-ATP; the non-labeled strands were phosphorylated with non-radioactive ATP. 10nM radioactively labeled, thiouridine containing siRNA duplexes were incubated with 1 μM dsRBD1, 1 μM dsRBD2, 500 nM LoqsPD$_{\Delta NC}$, 500 nM LoqsPD or 250 nM Dcr-2/LoqsPD complex for 30 min at room temperature. Crosslinking was induced with 3 × 500 mJ/cm^2 of 365 nm wavelength light, and the samples were resolved on a 10 or 15% PAA gel for 1 h at 170 V. The radioactive signals were read out using a phosphorimager screen on a Typhoon imager and quantified using Multigauge V3.0 software.

Cell culture and deep sequencing experiments

Drosophila S2-cells were grown and transfected in Schneider's medium as described before (45). For genome editing, a cas9 expression plasmid was co-transfected with a PCR-generated sgRNA expression cassette. One week later, the cells were diluted, clones were picked, amplified and the induced mutations were characterized. Further details and oligonucleotide sequences are provided in the supplementary section. The cells were then treated with 300 ng/ml of dsRNA targeting *Renilla* luciferase, 100 ng/ml of dsRNA targeting firefly luciferase, 30 ng/ml of dsRNA targeting GFP and 10 ng/ml of dsRNA targeting DsRed. Total RNA was isolated 3 days later and processed for comparative Illumina sequencing with and without a β-elimination step as previously described (46). To compare the different sequencing datasets, a normalization to the sum of all miRNA-matching reads was performed. Further details on data analysis are given in the supplementary section.

RESULTS

R2D2 is dispensable for loading of siRNAs into Ago2 in Drosophila S2-cells

R2D2 was originally identified via co-purification with Dcr-2. Genetic analysis revealed that it is required for the loading, but not the production, of siRNAs in *Drosophila* embryos (8). Subsequent studies indicated that the PD isoform of Loqs, an R2D2 paralog involved in the endo-siRNA pathway, can also interact with Dcr-2 (47–49). Based on data obtained with mutant flies, a sequential model was proposed where Loqs-PD interacts with Dcr-2 during the dicing reaction while R2D2 is an obligatory partner during the loading reaction of all siRNAs (40,48,50,51). In S2 cells, however, R2D2 was dispensable for the function of endogenous siRNAs but required for full silencing activity of experimentally introduced dsRNA (52,53), thus arguing for the existence of an alternative RLC for endo-siRNAs (Supplementary Figure S1A).

To clarify whether this discrepancy was due to technical differences (depletion of factors via RNAi in cell culture vs. mutant alleles *in vivo*) we generated *r2d2* as well as *loqs* mutant cell lines via *CRISPR-cas9* mediated genome editing. Absence of the proteins was verified by sequencing of the mutated loci (data not shown) and western blotting (Supplementary Figure S1B and data not shown). We analyzed the small RNA content via deep sequencing, exploiting the fact that the 2′-*O*-methyl modified, Ago2-loaded siRNAs are resistant to oxidation by periodate (54,55) to determine their loading state. A comparison of the predominantly Ago1-loaded miRNAs (sensitive to oxidation and β-elimination) with Ago2-loaded transposon-targeting endo-siRNAs allows to assess the functionality of RISC loading complex. Strikingly, we found that both endogenous and exogenous siRNAs can be loaded normally in the complete absence of *r2d2*. When *loqs* was inactivated, however, the endogenous siRNAs were partially sensitive to β-elimination (Figure 1A). This effect was consistently observed in three independent experiments involving two distinct *loqs* and *r2d2* mutant cell clones (Supplementary Figure S2). Based on the axis intercept of trendlines through the TE-matching endo-siRNA data points, we estimate that the amount of Ago2-loaded siRNAs was 3.5 ± 1.2 fold lower in *loqs* mutant cells (average ± SD, three biological replicates, Supplementary Figure S2A–C). The same was true for siRNAs derived from exogenously added dsRNA but not for Ago2-tropic miRNAs such as miR-276-5p or miR-277-3p (Supplementary Figure S2D). R2D2 is nonetheless required for full efficiency of experimental RNAi in S2-cells (52), indicating that the two paralogs can function redundantly in siRNA loading. The remaining transposon-targeting siRNAs in either mutant showed no difference in the average ΔΔG (around 1 kcal/mol in all cases, range was from 0.90 to 1.05 kcal/mol). Furthermore, the 5'-nucleotide bias was essentially the same (∼38% U, ∼29%A, ∼13%G and ∼20%C) for all genotypes. We conclude that the remaining transposon-targeting endo-siRNAs are bona fide Ago2 loaded, consistent with our 2'-*O*-methylation state analysis.

While *loqs* is required to silence a transgene-derived endo-siRNA reporter, *r2d2* is required for silencing by the preferentially Ago2-loaded miR-277 (Supplementary Figure S1C). Thus, S2-cells apparently have two partially redundant RISC loading complexes: Dcr-2/R2D2 and Dcr-2/Loqs-PD.

Loqs dsRBDs bind dsRNA independently

It has been difficult to study the biochemical and structural properties of the dsRBD-containing RLC component in the past because recombinant production of R2D2 is challenging in the absence of Dcr-2. Fortunately, we could express Loqs-PD as well as its individual dsRNA binding domains. Fluorescence anisotropy measurements were performed to determine the binding affinity of the Loqs dsRBDs to various RNA substrates (Figure 1B, Supplementary Figure S3A). The sequence of our model substrates is derived from the *Drosophila* miRNA *bantam*, which was modified to mimic an siRNA duplex (21-nt siRNA duplex with 2 nt 3′ overhangs, 23 nt strand length, which will be termed *ban*-siRNA in the following) and a longer dsRNA

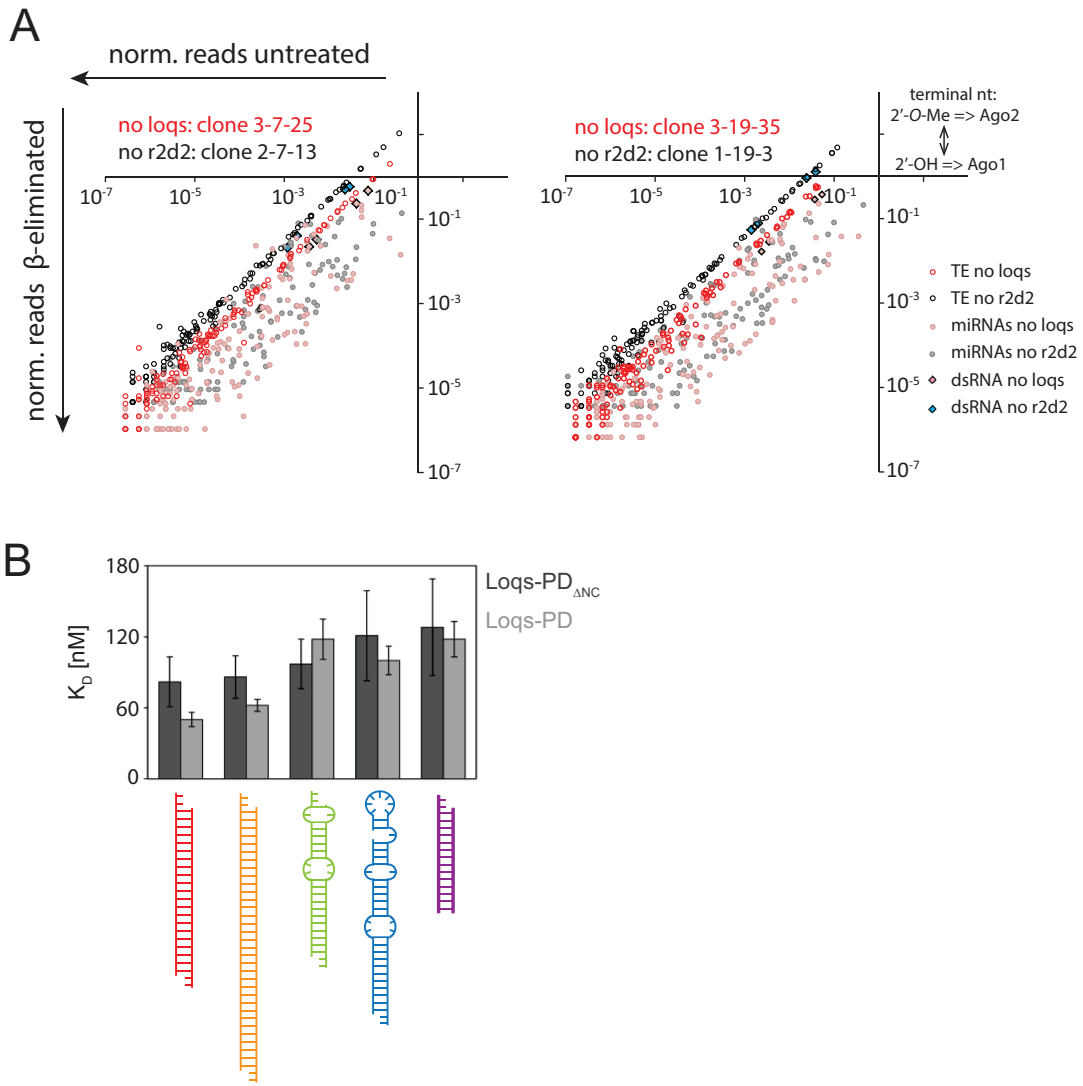

Figure 1. The PD isoform of Loqs is of central importance for siRNA biogenesis in S2-cells. (**A**) Small RNA sequencing libraries were created from genomically engineered S2 cell lines lacking either *r2d2* (lines 1-19-3 and 2-7-13, black or grey) or *loqs* (lines 3-19-35 and 3-7-25, red or pink). For both cell lines, libraries were generated directly from total RNA and after oxidation/beta-elimination to assess Ago2 loading state. Small RNAs were summed up for each transposon consensus sequence (open circles, transposon sequences can be several kb long) or miRNA (filled circles). Transposon-targeting endo-siRNAs and siRNAs derived from exogenously added siRNAs remained preferentially Ago2-loaded (= separated from miRNAs) in the absence of *r2d2* whereas the absence of *loqs* reduced their association with Ago2. The *loqs* mutation leads to a mild reduction in mature miRNA and siRNA levels because of its role during the nucleolytic processing steps (Dcr-1/Loqs-PB and Dcr-2/Loqs-PD complexes). These effects affect miRNAs and siRNAs comparably, though (see also Supplementary Figure S2) and are thus compensated in the miRNA-normalized data shown here. (**B**) Binding affinities for recombinant Loqs-PD$_{\Delta NC}$ (dark gray) and full-length Loqs-PD (light gray) determined by fluorescence anisotropy measurements for different RNA substrates; see Table 1 for the binding affinities and Supplementary Figure S3A for titration curves.

(35 nt strand length). The individual dsRBDs bind their substrates with comparable affinities (Supplementary Figure S3B and Tables 1 and 4). There is no pronounced difference in binding affinity between the different RNA constructs, which represent both the substrates and the products of dicing reactions (see supplement for further information).

The RNA binding region of Loqs proteins comprises the tandem dsRBDs, which are connected by a 45-residue linker (Loqs$_{\Delta NC}$). When comparing the binding of single and tandem dsRBDs only a moderate increase in binding affinity is observed. The gain in affinity is ~3-fold for the construct containing only the two domains connected via the linker and ~5-fold for full-length Loqs-PD (Table 1). The increase in affinity for the two dsRBDs together is clearly less than expected for additive binding, which should have led to a sub-picomolar affinity based on our measurements for the single dsRBDs (56). We thus conclude that RNA binding does not involve concomitant engagement of the two dsRBDs, which rather appear to bind independently to the RNA.

Table 1. Binding affinities determined by fluorescence anisotropy [nM]

RNA	Loqs dsRBD1	Loqs dsRBD2	$Loqs_{\Delta NC}$	Loqs-PD
siRNA	228 ± 27	278 ± 24	82 ± 21	50 ± 6
dsRNA	191 ± 29	229 ± 48	86 ± 18	62 ± 5
miRNA	233 ± 17	241 ± 75	97 ± 21	118 ± 17
pre-miRNA	221 ± 43	218 ± 61	121 ± 38	100 ± 12
14 ntRNA	365 ± 62	334 ± 8	128 ± 41	118 ± 15

Loqs dsRBDs adopt a dsRBD fold with a canonical RNA binding interface

To analyze molecular details of the LoqsPD-dsRNA interaction we determined the structures of the first and second dsRBD, which are common to all Loqs isoforms (Supplementary Figure S1A). NMR ^{1}H,^{15}N-correlation spectra of the single domains superimpose very well with those of Loqs-$PD_{\Delta NC}$ (Supplementary Figure S4A). This demonstrates that the individual dsRBDs do not strongly interact in solution in the absence of RNA, and is consistent with NMR ^{15}N relaxation data (Supplementary Figure S4B). $\{^{1}H\}$–^{15}N heteronuclear NOE data (Figure 2B) indicate that the two domains are connected by a flexible linker (residues 206–251) that allows the domains to tumble independently in solution. The structures of the two dsRBDs were determined using ROSETTA and the NOE-based RASREC-ROSETTA protocol (57). Structural statistics are shown in Table 2. Both dsRBDs exhibit the canonical αββββα-topology (15,16) with two helices packed from one side onto a triple-stranded β-sheet connected by short flexible loops (Figure 2A and C).

To map the RNA binding interface on the dsRBDs we performed NMR titrations with unlabeled RNA to ^{15}N-labeled single dsRBD1 and dsRBD2 domains as well as the tandem domain construct Loqs-$PD_{\Delta NC}$. Significant changes in NMR chemical shifts are observed upon addition of a *ban*-siRNA (Figure 3A and B). Mapping of the NMR chemical shift perturbations (CSPs) onto the structures shows that three regions are involved in dsRNA binding: the two helices (α_1, α_2 and α_3, α_4 in dsRBD1 and dsRBD2, respectively), and the loops connecting strands β_2–β_3 and β_5–β_6, respectively, in each domain (Figure 3C). Similar CSPs are observed upon titration of single domains or the tandem domain (Figure 3B), confirming that both domains interact individually with the RNA with the canonical binding surface. Importantly, the NMR titrations demonstrate that the linker connecting dsRBD1 and dsRBD2 remains flexible and does not mediate contacts to the RNA.

Loqs-PD slides along the siRNA duplex with preferential binding at the siRNA termini

Based on our analysis of S2-cell RNA (Figure 1A) we expected that the Dcr-2/Loqs-PD complex can perform a similar function as the Dcr-2/R2D2 complex, which interprets the difference in base-pairing stability at either end of the siRNA (32). To test this hypothesis, we employed 4-thio-uridine labeled synthetic RNA substrates to allow site-specific protein–RNA cross-links. We created a series of substrates that report protein binding along the entire siRNA molecule (Supplementary Figure S5A). For both Loqs-$PD_{\Delta NC}$ and full-length Loqs-PD, we found that the cross-linking efficiency is higher at either end of the RNA duplex than in the center; this was true even when the corresponding mismatch-containing miRNA/miRNA* duplex was used (data not shown). In this assay, a clear preference for the more stably base-paired end of the duplex was not detected at any of the interrogated positions (Figure 4A), perhaps due to the fact that the thermodynamic asymmetry of this model duplex is moderate as A–U versus G–C base pair differences occur only at the fifth position. The same cross-linking profile was observed for the individual dsRBDs (Supplementary Figure S5B).

The current model for the Dcr-2/R2D2 RLC postulates that R2D2 initiates strand selection by binding to the more stably base-paired end, although the molecular mechanism for this is unknown. To explore whether the Loqs-PD subunit of the alternative RLC may have an intrinsic preference for the more stably base-paired siRNA we analyzed intermolecular NMR paramagnetic relaxation enhancements (PREs). PREs were measured by the attachment of a paramagnetic TEMPO spin label separately to either 5′ end of the RNA duplex (58,59). The spin label causes distance-dependent line-broadening of NMR signals within a range of up to ≈20 Å distance and the resulting PREs thus report on spatial proximity between protein and the RNA-attached spin label. PRE measurements are more sensitive to detect weak differences (60,61) than the biochemical approaches using site-specific cross-linking. PREs were measured by comparing ^{1}H,^{15}N correlation NMR experiments of the Loqs-$PD_{\Delta NC}$ protein bound to *ban*-siRNA with terminally attached TEMPO spin labels in the paramagnetic and diamagnetic state (58). Moderate intermolecular PREs are observed for several protein residues (R187, K299, H310) when the spin label is attached to the more stably base-paired end of the RNA (G1 in Figure 4B, Supplementary Figure S6A), indicating a stronger interaction with this region of the RNA duplex. In contrast, only very weak PRE effects are detectable in similar regions when a spin label is attached to the less stably base-paired end (G24 in Figure 4B, Supplementary Figure S6A). To further support this conclusion, we designed an siRNA duplex with a very pronounced thermodynamic asymmetry (Figure 4C, Supplementary Figure S6B). Compared to the *ban*-siRNA this highly asymmetric duplex shows substantially increased PRE effects to the more stable end of the RNA duplex, thus supporting the notion that the dsRBDs sense the thermodynamically more stable regions of a RNA helix. These data demonstrate that Loqs-PD is not bound with comparably affinity to the two termini of the RNA duplex but has a small, but notable intrinsic preference to bind to the more stably base-paired end.

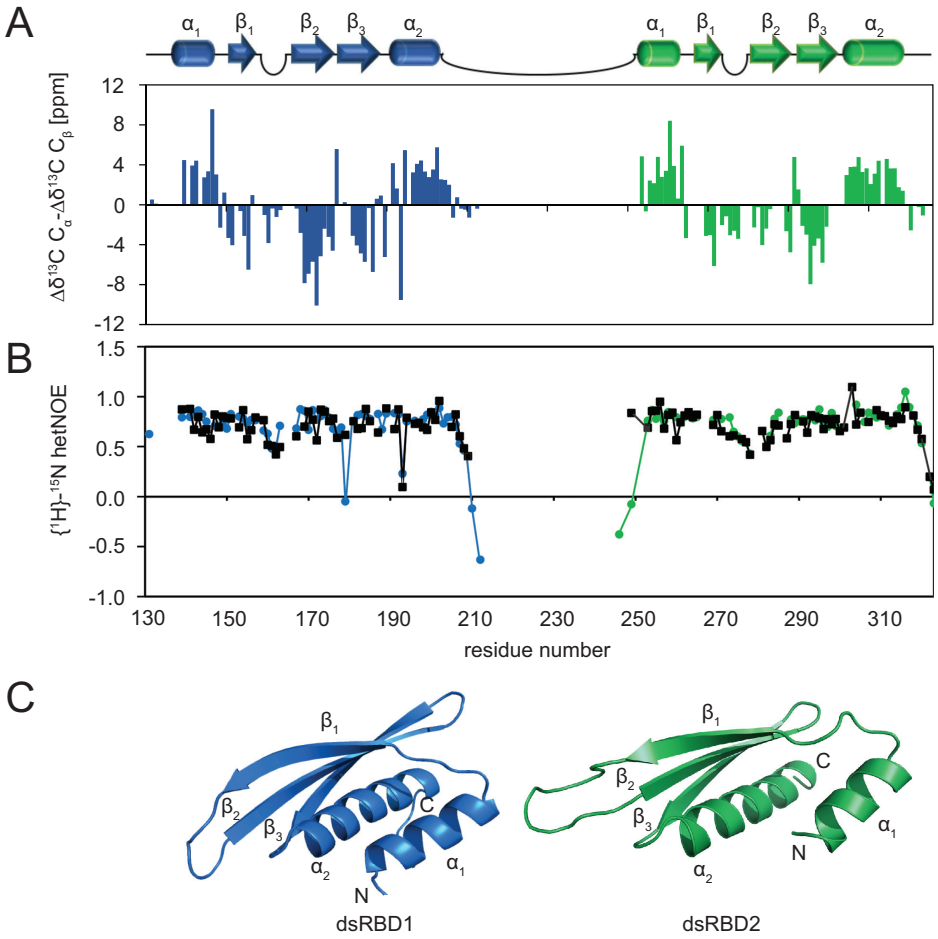

Figure 2. NMR analysis and structures of Loqs dsRBD1 and dsRBD2. (**A**) NMR ^{13}C secondary chemical shifts ($\Delta\delta^{13}C_\alpha$-$\Delta\delta^{13}C_\beta$) of the single domains (dsRBD1 in blue, dsRBD2 in green) indicate that both Loqs dsRBDs exhibit the conserved αββββα topology. Secondary structure elements are depicted as cartoons on top. (**B**) Low $\{^1H\}$–^{15}N heteronuclear NOE data show that the linker connecting dsRBD1 and dsRBD2 is highly flexible in solution. Specific loops that contribute to RNA binding in the two dsRBDs also exhibit some flexibility. Data for single domains are shown in black, data for the tandem construct are colored in blue (dsRBD1) and green (dsRBD2). (**C**) The NMR-derived structures show that the Loqs dsRBDs adopt a canonical dsRBD fold. Ensembles of the 10 lowest energy structures are shown in Supplementary Figure S4C.

Table 2. Structural statistics for the NMR structures of dsRBD1 and dsRBD2

	dsRBD1 (aa 137-205)	dsRBD2 (aa 215–318)
Rosetta structural statistics		
NOEs		
With unique assignment		887
With intra-residue assignment		559
With sequential assignment $\|i-j\|=1$		180
With medium-range assignment $1<\|i-j\|<5$		52
With long-range assignment $\|i-j\|>5$		96
Eliminated due to distance violations		89
Eliminated due to network, minimal peak volume and maximal assignments		81
Coordinate precision r.m.s.d. [Å][a]		
Backbone	2.12	1.04
Heavy atom	8.46	5.79
Ramachandran statistics [%][b]		
Favored regions	99.3	96.8
Allowed regions	0.6	3.1
Outlier regions	0.1	0.2

[a]From SuperPose (77)
[b]Calculated with RAMPAGE, de Bakker *et al.* (78)

Table 3. SAXS data of Loqs-PD$_{\Delta NC}$, linker mutants and protein–RNA complexes

Sample	R_g [Å]	D^{max} [Å]	Porod [Å^3]
Loqs-PD$_{\Delta NC}$ 2.5 mg/ml	26.94 ± 0.46	91.9	34156.2
Loqs-PD$_{\Delta NC\Delta 21}$ 2.4 mg/ml	22.65 ± 1.03	78.7	26153.6
Loqs-PD$_{\Delta NC\Delta 41}$ 9.3 mg/ml	21.20 ± 0.20	72.6	25538.6
Loqs-PD$_{\Delta NC}$ 2.0 mg/ml + *ban*-siRNA	32.69 ± 0.48	114.4	56691.6
Loqs-PD$_{\Delta NC\Delta 21}$ 1.8 mg/ml + *ban*-siRNA	24.17 ± 0.40	84.29	38595.9
Loqs-PD$_{\Delta NC\Delta 31}$ 1.3 mg/ml + *ban*-siRNA	21.61 ± 0.30	75.34	23990.9

Table 4. Hill coefficients obtained from fitting the fluorescence anisotropy data

RNA	Loqs dsRBD1	Loqs dsRBD2	Loqs$_{\Delta NC}$	Loqs-PD
siRNA	7.9 ± 3.0	3.4 ± 2.1	3.3 ± 0.9	1.3 ± 0.2
dsRNA	3.9 ± 1.0	3.0 ± 1.2	3.2 ± 0.8	2.5 ± 0.2
miRNA	5.1 ± 1.6	3.8 ± 1.6	5.1 ± 2.9	3.3 ± 0.8
pre-miRNA	4.5 ± 0.8	2.6 ± 0.7	4.6 ± 0.9	2.4 ± 0.7
14 ntRNA	7.7 ± 2.4	2.0 ± 1.7	3.9 ± 1.0	2.9 ± 0.7

We compared imino NOESY and ^{1}H,^{15}N imino correlation spectra of the free and protein-bound RNA to map the Loqs-PD binding on to the siRNA duplex. Upon addition of unlabeled Loqs-PD$_{\Delta NC}$ protein all NMR signals from the observed isotope-labeled RNA show severe line broadening (Figure 5A). Imino NMR signals of several guanine and uracil bases could still be traced, while all uracil imino signals in the U-rich central region (U33, U34) are broadened beyond detection (Figure 5A). This likely is an indication of sliding of the protein along the double-helical RNA duplex, where varying chemical environments in the different dynamically exchanging binding modes cause line-broadening. The NMR chemical shift perturbations thus demonstrate that Loqs exhibits a highly dynamic binding to the dsRNA that involves sliding along the RNA duplex.

Dynamic siRNA recognition by the Loqs-PD tandem dsRBDs

To explore whether the linker plays a role for the dynamic siRNA recognition, we prepared Loqs-PD$_{\Delta NC}$ mutants with varying linker lengths (Δ11, Δ21, Δ31, Δ41) connecting the two dsRBDs (Supplementary Figure S7A). Potential interactions of the dsRBDs where analyzed by comparing NMR chemical shifts in ^{1}H,^{15}N correlation spectra (Figure 5B, Supplementary Figure S7B). Analysis of the linker deletion tandem domains in the absence of RNA shows only negligible changes in the chemical shifts of the individual domains. However, an almost complete deletion of the linker (Δ41) leads to more pronounced effects on the NMR spectra indicating that the relative domain arrangement is affected, presumably by steric strain. A significant compaction with decreasing linker length is also indicated by SAXS analysis (Supplementary Figure S7D). When bound to siRNA, the protein–RNA binding interface is not much affected by shortening of the linker as similar chemical shift perturbations are observed upon RNA binding independent of the linker length. Nevertheless, a gradual shortening of the linker leads to increased line broadening, which suggests more pronounced sliding of the protein on the dsRNA ligand (Figure 5B and C, Supplementary Figure S7B and C). Most likely, the protein with a shortened linker cannot adopt a domain arrangement required for optimal RNA contacts of both domains and switches thus to a dynamic binding mode where sometimes only one of the dsRBDs may be bound to the RNA. Consistent with this fluorescence anisotropy experiments show that the binding affinity of the Δ41 linker deletion with our dsRNA model substrates exhibits a two-fold reduction compared to the wild type linker, and is thus comparable with a single dsRBD (Table 1; Supplementary Figure S7F).

To characterize the overall shape of the protein–RNA complex we compared SAXS experiments for the free tandem dsRBD protein Loqs-PD$_{\Delta NC}$, the free *ban*-siRNA and a complex of the two (Figure 5D; Table 3). The SAXS data for the unbound Loqs-PD$_{\Delta NC}$ indicate a maximum dimension of ≈100 Å (Figure 5D). This distance is consistent with the presence of an unstructured linker, where the two domains are flexibly connected. The dynamic arrangement of the two dsRBDs in the free protein is further confirmed by SAXS data for the Loqs linker mutants (Supplementary Figure S7D; Table 3), where the maximum distance decreases proportional with shortening of the linker.

SAXS data of the protein–RNA complex indicate a maximum distance of ≈115 Å. This is consistent with the preferential binding of the two dsRBDs to the termini of the siRNA duplex, for which a pairwise distance of ≈110 Å is expected (Figure 5E). Interestingly, upon truncation of the linker connecting the tandem dsRBDs in the protein–RNA complexes the dimension of the complex as indicated by SAXS decreases accordingly (Supplementary Figure S7E). This is consistent with a dynamic binding and sliding of the two dsRBDs on the dsRNA helix, where shortening of the linker will restrict the spatial separation of the two domains. The combined analysis of the NMR and SAXS data shows that both dsRBDs exhibit a dynamic binding mode that involves sliding along the dsRNA helix, and preferentially reside at the siRNA termini.

We also analyzed whether the linker is important for the interaction of Loqs-PD with Dcr-2. For this, we transfected a myc-tagged version of Loqs-PD $_{\Delta 41}$ into an S2-cell clone harboring a genomically integrated Flag$_2$-tag at the C-terminus of Dcr-2 (62). Then, we immunoprecipitated the endogenous Dcr-2 protein and confirmed by Western blot that myc-Loqs-PD$_{\Delta 41}$ was still associated with Dcr-2 (Sup-

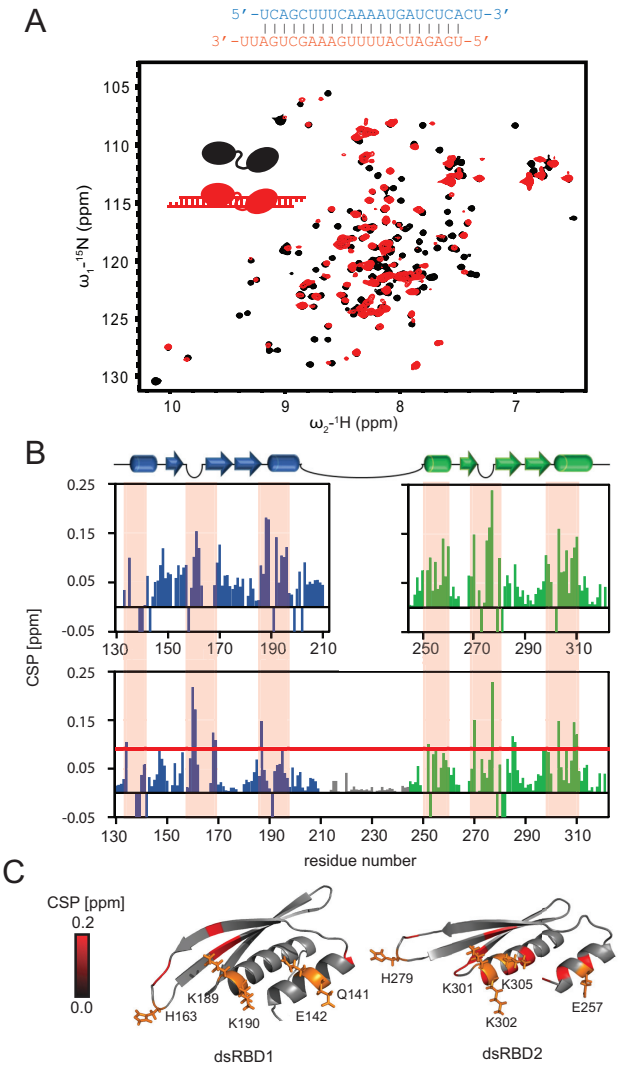

Figure 3. Loqs dsRBD1 and 2 bind siRNA independently and via conserved binding mode. (**A**) $^{1}H,^{15}N$ correlation NMR spectra of Loqs-$PD_{\Delta NC}$ free (black) and bound to *ban*-siRNA (red), the RNA sequence is shown above. (**B**) Upon titration of *ban*-siRNA the amide signals in the tandem dsRBD protein exhibit significant chemical shift perturbations (CSP), while the linker (gray) is not affected. The single domains titrated with the same RNA (graphs on top) show a similar pattern of CSP demonstrating that both domains bind RNA independently. Negative bars indicate broadened lines and non-traceable signals. Residues with CSP above the red line (mean ± SD) are highlighted in C. The orange shaded boxes indicate main RNA binding regions. (**C**) The CSP induced by RNA binding are plotted on the domain structures and reveal three binding regions: The first helix (α_1, α_3), the loop (L_1, L_2) and the N terminal part of the second helix (α_2, α_4) are involved in RNA binding. Loqs thus binds via the typical dsRBD interface. Side chains of typical conserved RNA binding residues are shown as orange sticks. We confirmed that the Loqs dsRBD1 and dsRBD2 mediate canonical interactions with the dsRNA by similarity searches using DALI (77). Both Loqs dsRBDs superimpose well with dsRBD-dsRNA complex structures from the respective top hits (Supplementary Figure S4D, Supplementary Table S1).

plementary Figure S7G). In summary, we conclude that the inter-domain linker enables simultaneous tandem-dsRBD binding of Loqs-PD. Interaction with Dcr-2, on the other hand, is independent of the linker.

Loqs-PD and Dcr-2 together can interpret the thermodynamic asymmetry of an siRNA

The NMR data indicate only a very small binding preference towards the thermodynamically more stable end of the siRNA. We therefore investigated the role of Dcr-2 for guide strand selection. First, we used recombinant Dcr-2 and cross-linked it to our siRNA model substrates. Unlike previous publications (32,33) we were able to observe crosslinking of Dcr-2 alone to our oligonucleotide substrates. Like Loqs-PD, Dcr-2 showed more efficient crosslinking to the ends of the siRNA duplex and we did not detect a preference for the less stably base paired end of our moderately asymmetric siRNA (Figure 6A). In contrast, upon addition of a 1.5–2-fold excess of full-length Loqs-PD over Dcr-2 to the binding reaction, asymmetric binding of Dcr-2 with a preference for the less stably base-paired end was induced (Figure 6A). This capacity does not reflect competitive displacement from the more stably base-paired end as it requires protein–protein interaction between Dcr-2 and Loqs-PD: The double-domain construct Loqs-$PD_{\Delta NC}$ that lacks the C-terminal 37 amino acids involved in the association with Dcr-2 (47,52) was unable to induce preferential binding of Dcr-2 to the less stably base paired end of the siRNA (Figure 6A). Thus, the alternative RISC loading complex has properties that differ from each of its subunits alone.

Why can the hetero-duplex of Dcr-2 and a dsRBD protein sense the differential base pairing stability at the siRNA ends so efficiently? Since the two proteins must engage in a protein–protein interaction for this purpose, it may be that RLC induces bending or torsion of the RNA double helix, and that this is more easily accommodated with Dcr-2 bound to the less stably base-paired end. A similar communication via double-stranded nucleic acids has recently been described for proteins bound to DNA (63,64). An siRNA with a nick between positions 11 and 12 of the passenger strand should reduce the transmission of bending or torsion from one siRNA end to the other. Yet, this molecule was bound with identical affinity as the normal siRNA by the Loqs dsRBDs (Supplementary Figure S5C) and asymmetric binding of the Dcr2–LoqsPD complex to the nicked siRNA duplex was retained (Figure 6B). Thus, propagation of RNA conformational changes along the RNA duplex is not essential for guide strand selection.

DISCUSSION

The siRNA duplexes used to trigger RNA interference are structurally symmetric but one of the two strands can become preferentially incorporated into RISC. This functional asymmetry is determined by the relative base-pairing stability at either end of the siRNA duplex (27,28). Incorporation of this concept into siRNA design rules is now essential for every knock-down experiment, yet we do not fully understand the molecular mechanisms behind it. Functional characterization of the *Drosophila* Dcr-2/R2D2

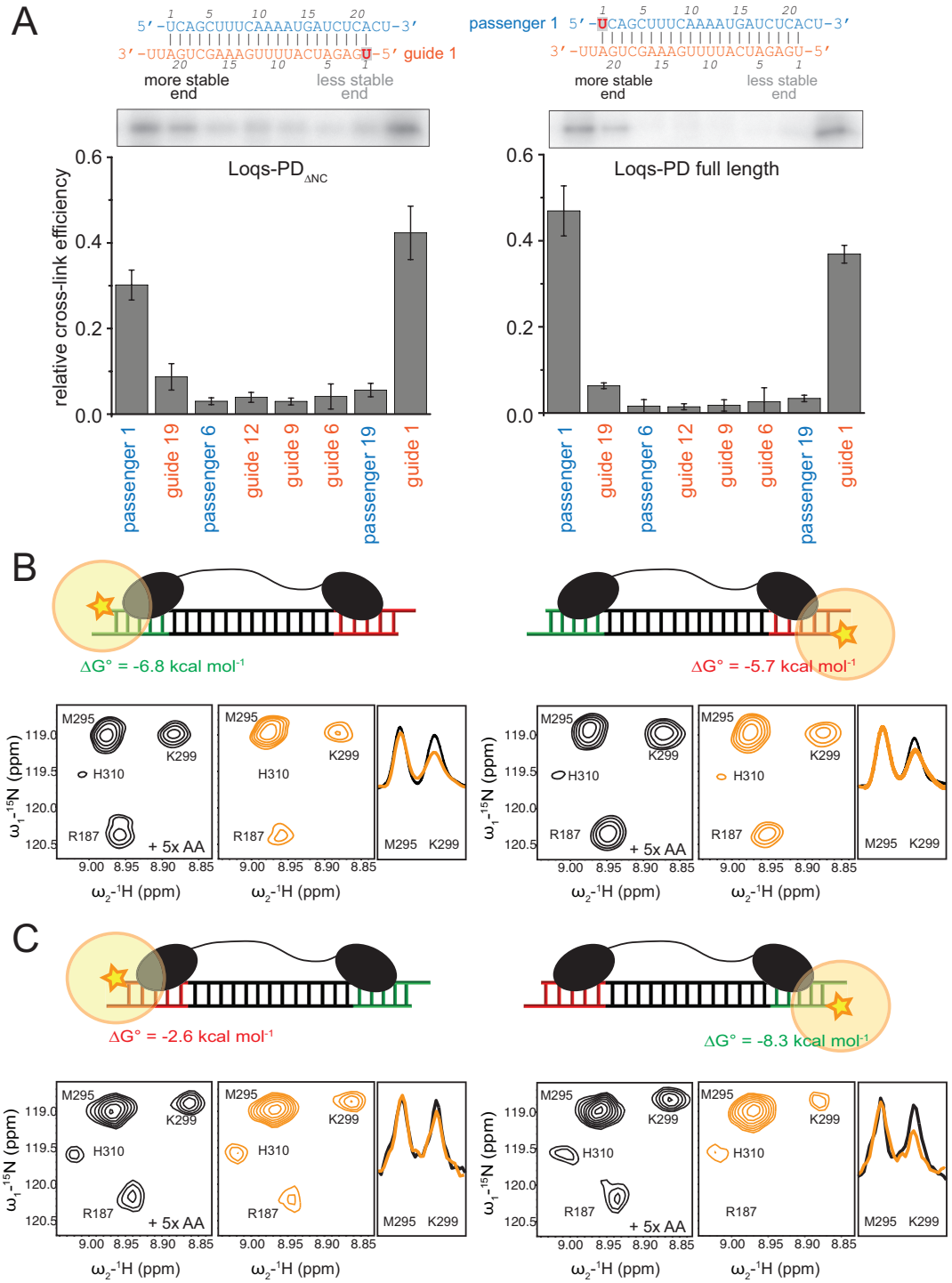

Figure 4. Loqs-PD preferentially resides at the termini of a duplex siRNA. (**A**) Site-specific cross-linking experiments were carried out with site-specifically 4-thio-uridine labeled RNAs (see Supplementary Figure S5 for further details). The RNAs were radioactively labeled, incubated with recombinant protein, cross-linked with 365 nm UV light and separated by gel electrophoresis. Both full-length Loqs-PD and Loqs-PD$_{\Delta NC}$ preferentially react with labeled uridine-residues at either end of the dsRNA. The bar graphs represent a quantitative analysis of three independent experiments (mean ± SD). (**B**) Intermolecular paramagnetic relaxation enhancements (PREs (Supplementary Figure S6A) observed in ^{1}H,^{15}N HSQC NMR spectra with ^{15}N-labeled Loqs-PD bound to an RNA duplex with a TEMPO-spin label (orange star in the schematic pictures) attached to either the more stable (left) or the less stable (right) 5′ end. Zoomed views of NMR spectra in the diamagnetic and paramagnetic state, are shown in black and orange, respectively. A stronger reduction in signal intensities for the paramagnetic state observed on the left indicates a preferential binding to the more stable end of the siRNA. For the M295 and K299 amide 1D traces taken from the 2D spectra are shown on the right to demonstrate the PRE-induced line-broadening. (**C**) Intermolecular PREs observed for a highly asymmetric RNA. Note, that the thermodynamic stability of this RNA duplex is inverted compared to (B). The significantly stronger PRE effects observed relate to the larger thermodynamic asymmetry of the duplex. The RNA sequence and experimental PRE data are shown in Supplementary Figure S6B.

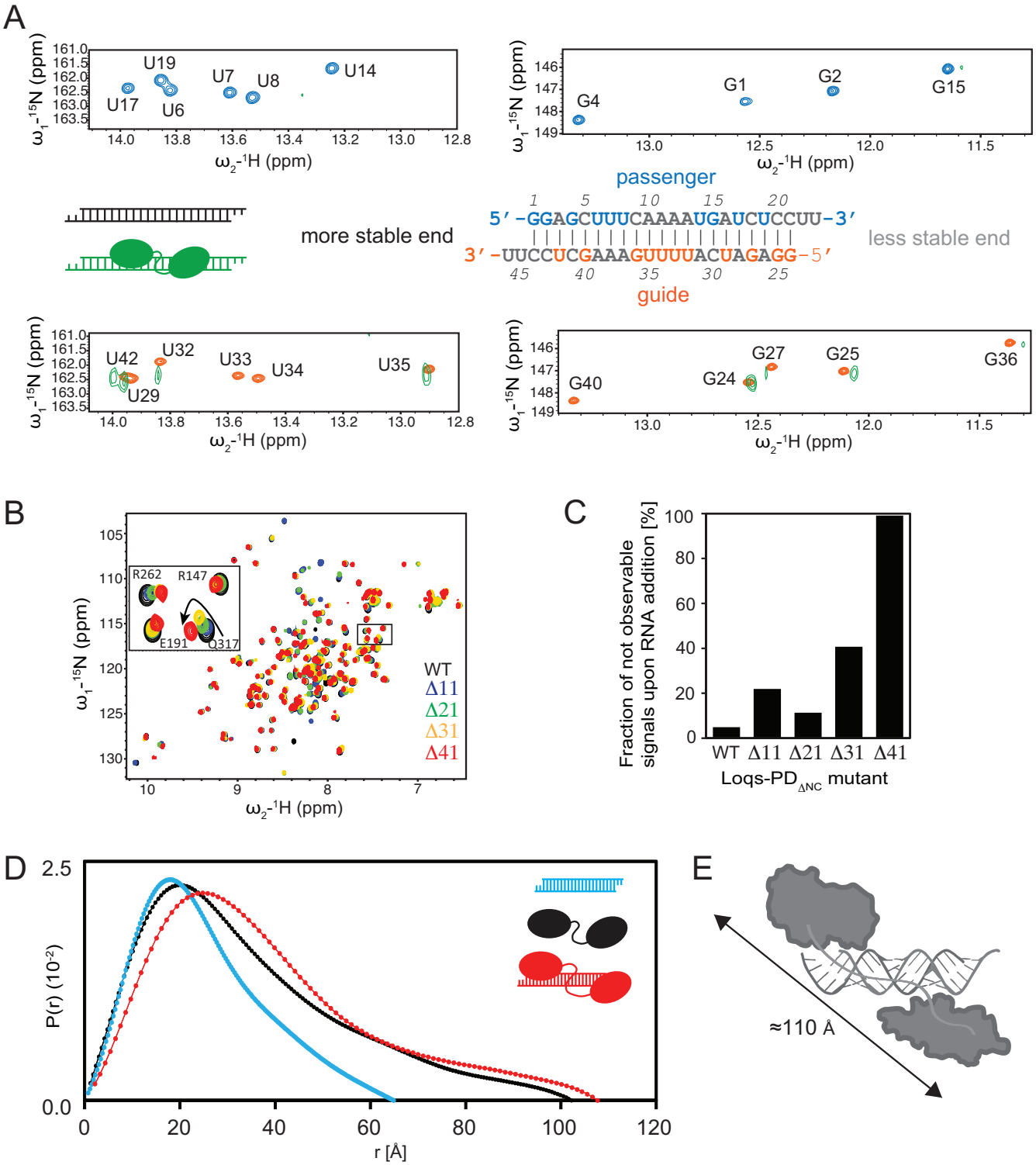

Figure 5. Loqs slides along RNA and the linker is needed for proper domain arrangement. (**A**) Zoomed view of ^{1}H,^{15}N NMR correlation spectra of the imino region of the *ban*-siRNA in the free (blue and orange, depending on which RNA strand is isotope-labeled and thus NMR observable) and protein-bound (green) form. Imino signals in the less stable 5′ region (i.e. residues 15–23 in the passenger and 24–36 in the guide strand) experience less line-broadening (reflecting weaker interactions with the protein) than those in the more stable end. The line-broadening observed indicates sliding of the protein along the RNA. Note, that only bases (G, U) with imino protons are detectable, while A and C bases are not detectable in this experiment and are therefore shown in light gray in the secondary structure of the RNA. (**B**) Superposition of ^{1}H,^{15}N HSQC NMR spectra of wildtype Loqs-PD$_{\Delta NC}$ free (black) and linker mutants as indicated by different colors. The zoomed view shows that shortening of the linker leads to chemical shift changes along a linear trajectory, while a complete deletion of the linker causes strong chemical shift changes in a different direction (red), indicating significant structural perturbation or rigidification of the domain arrangements in the tandem dsRBDs upon linker deletion. (**C**) The fraction of unobservable NMR signals in ^{1}H,^{15}N NMR correlation spectra in the presence of RNA for tandem dsRBD proteins, wildtype and with different linker deletions is shown. (**D**) SAXS-derived pairwise distance distribution P(r) for siRNA (blue), Loqs-PD$_{\Delta NC}$(black) and the 1:1 complex (red).

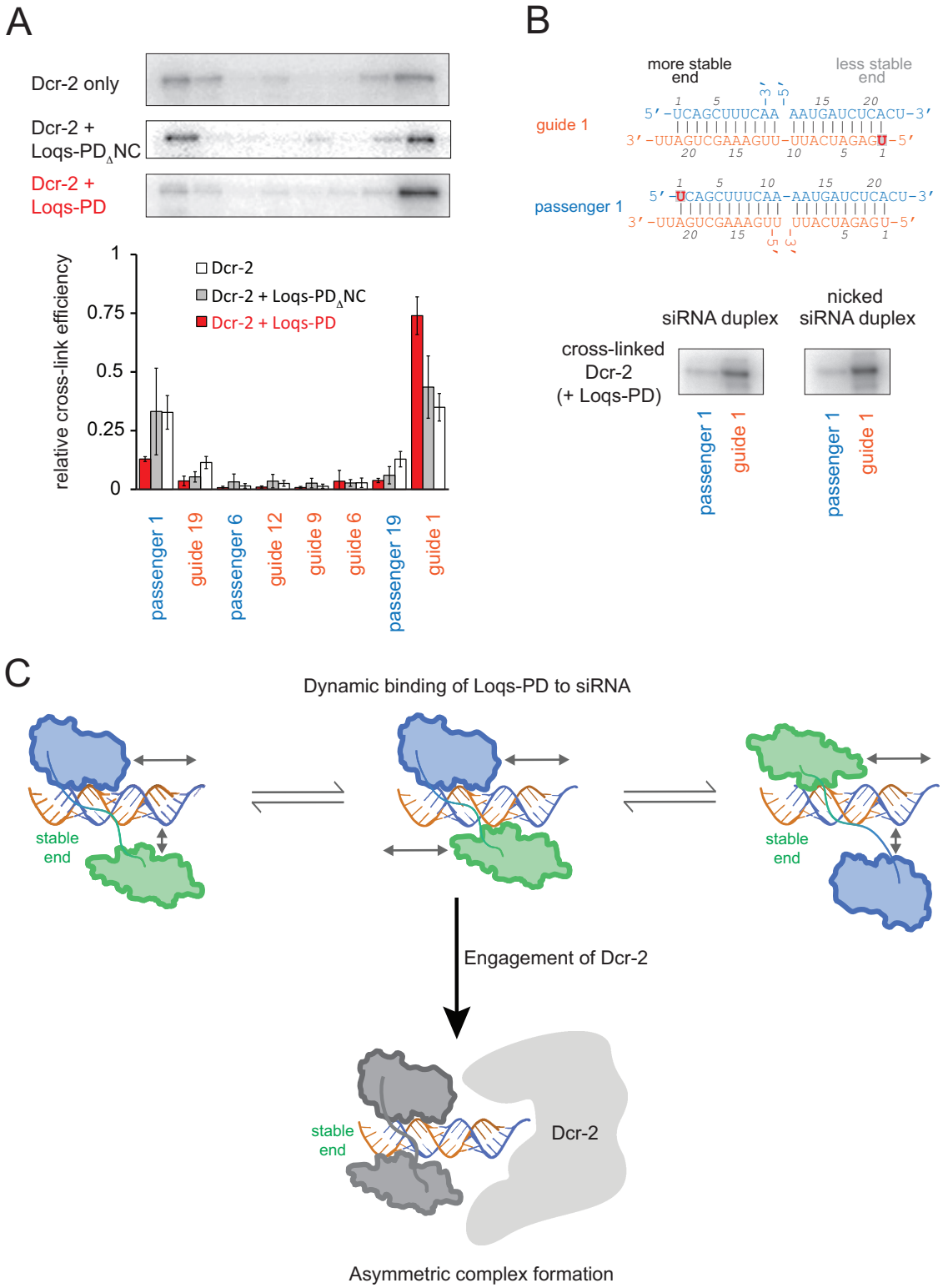

Figure 6. Dcr-2 and Loqs-PD can interpret the thermodynamic siRNA asymmetry. (**A**) Site-specific cross-linking of Dcr-2 to 4-thio-uridine containing, radioactively labeled siRNAs revealed preferential association of Dcr-2 with the ends of a *ban*-siRNA; however, only the complex of full-length Loqs-PD with Dcr-2 can interpret the differential base-pairing stability at either end. The autoradiographs show cross-linked Dcr-2 protein, the bars below are a quantification of three independent experiments (mean ± SD). (**B**) To test whether the asymmetry sensing is communicated via distortions along the dsRNA helix, we created nicked siRNA duplexes (depicted on top) and cross-linked the Dcr-2 / Loqs-PD complex to either end. We could not detect any difference between the normal and the nicked siRNA duplex. (**C**) The dsRBD protein moiety of RLC (either Loqs-PD or R2D2) contributes to strand selection by identifying the more stably base-paired end. This may be facilitated by a prolonged sampling period, during which the dsRBD protein steps along the siRNA until Dcr-2 also engages in binding and fixes asymmetric complex formation

RISC loading complex (35,65) provided the first protein entity capable of interpreting the differential base pairing stability at the ends of an siRNA (32). Since Dcr-2 alone cannot fulfill this task, R2D2 was proposed to confer asymmetric binding of RLC on the siRNA (32). However, the individual contribution of R2D2 has been difficult to assess because it is degraded in the absence of Dcr-2 and recombinant production is challenging. Here, we employed genome engineering to demonstrate that the PD-isoform of Loqs, a homolog of human TRBP, forms an alternative RLC (aRLC) with Dcr-2 that is required to load transposon-targeting endo-siRNAs into Ago2 in cultured cells. We could recombinantly express Loqs-PD, enabling us to examine its function with structural and biochemical approaches. Our results indicate that the two double-stranded RNA binding domains associate independently of each other with RNA. This is possible as the tandem dsRBDs are connected via a long, unstructured linker region that uncouples their behavior in solution. Analysis of imino NMR signals in the RNA indicates a highly dynamic binding mode, which may be required to search and scan the RNA double helix. Truncation or deletion of the flexible linker perturbs the tandem dsRBD binding mode. Site-specific crosslinking confirms that the two proteins form an alternative RISC loading complex, which is able to interpret the asymmetry of the base-pairing stability at the termini of an siRNA. Importantly, our NMR data indicate that Loqs-PD has a moderate but notable intrinsic ability to recognize the more stably base-paired end of an siRNA duplex. This likely reflects that a more stable RNA helical confirmation provides an optimal binding surface for dsRBD binding. Our results therefore indicate a molecular mechanism for initiation of the strand selection process via asymmetry sensing by the dsRBD subunit of the RLC. Nevertheless, this preference is greatly enhanced in the protein complex with Dcr-2.

Does the alternative RLC exist only in S2-cells?

Previous reports that define RLC for loading of Ago2 in *Drosophila* relied thus far exclusively on genetic and biochemical experiments with *r2d2* mutant flies. Yet, a genome-wide RNAi screen with three different reporter constructs in cell culture recovered neither *loqs* nor *r2d2* (53). Our genome editing and deep sequencing experiments in this manuscript clearly demonstrate that a redundant RLC activity linked to Loqs exists in S2-cells. This is consistent with data from a genome-wide screen of DNA-damage induced siRNA generation where only *loqs*, but not *r2d2*, was recovered as a candidate (66). Is the alternative RLC that we describe in S2-cells a particular idiosyncrasy of this cell line? Transposon-targeting endo-siRNAs were slightly sensitive to oxidation and beta-elimination (an indication of reduced 2′-*O*-methyl modification and thus reduced Ago2 loading) in *loqs-PD* mutants and some Ago2-loaded siRNAs remain even in *r2d2* null mutant flies (42,52), suggesting that alternative RLC also acts in flies at a low level. Possibly, the action of alternative RLC is influenced by the relative expression levels of Loqs-PD and R2D2; in this case, the importance of RLC and alternative RLC (aRLC) may vary between tissues and cell lines. An important question is whether the two forms of RLC, which clearly co-exist in S2 cells (Supplementary Figure S1C), display specificity for certain small RNA substrates. Both complexes can load endogenous and exogenous siRNAs into Ago2, indicating that the contribution of each RLC may be dictated by their relative abundance. Unfortunately, we were unable to derive double-mutant clones to test the extent of redundancy between Loqs-PD and R2D2 directly. Previously, we had found that exogenous siRNAs were partially dependent on R2D2 and that isoform-specific knock-down of Loqs-PD only increased the efficiency of experimental RNAi (52). Our knock-out cells do not recapitulate this difference. One cause for this may be the fact that we deleted all isoforms of Loqs, while the knock-downs were specifically targeting Loqs-PD. It is conceivable that in the absence of co-factors for Dcr-1 (i.e. Loqs-PB or Loqs-PA), some R2D2 is being sequestered. Alternatively, the growth time required in our genome editing procedure may select for cells that have undergone compensatory changes which are absent in the knock-down approach. In any case, however, the fact that exogenous RNAi is not completely abrogated upon loss of R2D2 is consistent in both approaches and clearly indicates that a redundant activity must exist.

RNA binding by the tandem dsRBDs of Loqs-PD

The assembly of multiple ligand binding sites on a single protein can lead to improved binding due to avidity effects and/or even cooperativity. This is exploited in both natural (e.g. oxygen transport by hemoglobin or bivalent binding by vertebrate antibodies) and synthetic (e.g. multimerization of epitope tags on proteins or transcription factor binding sites in promoters) biomolecular interactions. In multi-domain RNA binding proteins, various modes of RNA binding have been observed ranging from independent to preformed domain-domain arrangements (67–72). A flexible linker connecting two RBDs may thereby functionally uncouple the RNA binding contributions of individual domains (56). Here, we observed only a moderate increase in binding affinity when comparing the individual versus tandem Loqs-PD dsRBDs. Similar observations were made for the human homolog TRBP and several other, multiple dsRBD containing proteins (26). According to our deletion analysis, a minimal linker length is required in order for the two dsRBDs to functionally interact. Presumably, this is to accommodate the restraints imposed by the rigid, helical structure of dsRNA. Single molecule studies suggested that longer linkers, e.g. the 61 amino acid linker in TRBP, favor a binding mode that allows the protein to 'slide' along dsRNA whereas shorter linkers, e.g. the 25 amino acids in Staufen1, lead to a rather stationary binding (26). The task of Loqs-PD in aRLC is to provide a structure-specific recognition of short siRNA helices in a reversible manner to allow subsequent hand-over to the effector protein Ago2. Single-molecule experiments have revealed that the Loqs-PB isoform and its human homolog TRBP can slide along immobilized dsRNA (73). Our NMR data support these observations and show that binding of Loqs to dsRNA is dynamic in solution and involves sliding along the dsRNA helix. The native 45-residue interdomain linker length may thus constitute an optimal compromise

for sufficiently strong, yet mobile and reversible interaction with the duplex RNA.

Discrimination of the siRNA guide strand by dsRBD proteins

One of the most intriguing aspects of siRNA biogenesis is the identification of the guide strand based on the differential base pairing stability at either end (27,28). In the case of *Drosophila*, the RISC loading complex (RLC) composed of Dcr-2 and the dsRBD cofactor R2D2 can interpret the thermodynamic asymmetry (32). While it is a matter of debate whether loading of mammalian RISC with siRNAs requires the Dicer/TRBP complex for strand discrimination (34,38,39,74,75), it is clear that during human RISC assembly thermodynamic asymmetry is considered independent of other features, such as structural imperfections or terminal nucleotide identity (27). Noland and colleagues demonstrated that the human Dicer/TRBP complex or a fusion of human Dicer with the tandem dsRBDs from the spermatid perinuclear RNA binding protein (SPNR) can bind asymmetrically to siRNA duplexes. Further studies suggested TRBP to sense thermodynamic asymmetry on its own (36). Here, we could demonstrate that the complex of *Drosophila* Dcr-2 and Loqs-PD can also serve as a sensor for siRNA asymmetry and represents an alternative RLC. As for the human complex (33) efficient sensing depends on a protein–protein interaction between Dcr-2 and Loqs-PD. Evolution has thus produced distinct approaches for loading *Drosophila* Ago2. Nevertheless, the presence of a dsRBD partner protein for Dcr-2 is an essential and conserved requirement. Due to imperfect base-pairing in the precursors of microRNAs, their loading into Ago proteins may potentially be distinct from siRNA loading. Intriguingly, though, the dsRBD domains present in Loqs-PD are also present in the Loqs-PB isoform that partners with Dcr-1 for miRNA biogenesis.

Cross-linking of R2D2 to siRNA ends is influenced by the phosphorylation state of the 5′-end (32), indicating that recognition of siRNA ends may be possible for dsRBD proteins. A likely scenario is thus initial binding at a random position, followed by sliding (Figure 6C). Considering that an individual dsRBD covers a stretch of ∼12 bp on duplex RNA, this 'sliding' along an siRNA may rather represent a sequential engagement of either of the two dsRBDs and could also be envisaged as an oscillation between alternative binding states. Our NMR PRE data indicate that Loqs-PD has a weak preference to bind the more stably base-paired end, which is expected to be more rigid and represent a more canonical double-stranded RNA conformation. However, this preference appears too weak to explain the observed loading bias. Thus, an amplification mechanism exists upon formation of RLC together with Dcr-2. The NMR PRE data did not indicate a preference for a particular dsRBD in Loqs-PD to bind to the more stable base-paired end, arguing that the flexible linker indeed connects two functionally equivalent domains.

Taken together, we propose that after initial binding, a dynamic 'scanning' mode of RNA–protein association is established. In this mode, RLC slides or oscillates along the RNA duplex towards either end with the help of its tandem dsRBD subunit in a state that is not yet loading competent. Transition from the scanning mode to loading-competent RLC probably involves conformational changes in Dcr-2, perhaps equivalent to the state transitions described by Sinha and colleagues for the dicing reaction (76). Binding of the siRNA in the thermodynamically 'correct' orientation may prolong the RLC residence time, favor conformational transitions and thereby amplify the strand discrimination capability. In addition, a potential dimerization of aRLC as described for the TAF11/Dcr-2/R2D2 complex (37) may contribute to the selectivity. Finally, we cannot exclude that the Dcr-2 protein on its own also displays a weak preference for the less stably paired end, which was - like the binding preference of Loqs-PD - not detectable by our cross-link approach. Dynamic, solution-based assays may reveal if a weak preference also exists for Dcr-2 and, importantly, reveal how the strand discrimination ability is amplified during the RLC conformational transitions.

DATA AVAILABILITY

NMR chemical shifts, structural restraints and the atomic coordinate of dsRBD1 and dsRBD2 are deposited in the BMRB (accession 341244,34123) and the PDB (accession 5NPG, 5NPA), respectively. The sequencing data has been deposited at the European Nucleotide Archive (ENA) with the accession number PRJEB20483.

SUPPLEMENTARY DATA

Supplementary Data are available at NAR online.

ACKNOWLEDGEMENTS

We thank NMR time at the Bavarian NMR Center and SAXS measurements at the facility of the SFB1035 at Department Chemie, Technische Universität München.
Author Contributions: J.N.T. performed cloning, protein expression and RNA transcription and purification, NMR experiments and data analysis. S.F. performed binding assays and cell experiments. T.K. analyzed NMR spectra. R.S. performed SAXS measurements and data analysis. A.G. performed SLS measurements. C.W., M. J. and C.K. synthesized spin labelled RNA. R.B. and S.K. performed cell experiments and binding assays. O.L. and C.H. performed structure calculations. K.F. and M.S. designed the study. J.N.T., S.F., K.F. and M.S. wrote the manuscript. All authors discussed the results and commented on the manuscript.

FUNDING

Deutsche Forschungsgemeinschaft [SFB1035, GRK1721 to M.S., FO360/2, SFB646 to K.F.]. Funding for open access charge: Internal Funds.
Conflict of interest statement. None declared.

REFERENCES

1. van Rij,R.P., Saleh,M.C., Berry,B., Foo,C., Houk,A., Antoniewski,C. and Andino,R. (2006) The RNA silencing endonuclease Argonaute 2 mediates specific antiviral immunity in Drosophila melanogaster. *Genes Dev.*, **20**, 2985–2995.

2. Wang,X.H., Aliyari,R., Li,W.X., Li,H.W., Kim,K., Carthew,R., Atkinson,P. and Ding,S.W. (2006) RNA interference directs innate immunity against viruses in adult Drosophila. *Science*, **312**, 452–454.
3. van Mierlo,J.T., van Cleef,K.W. and van Rij,R.P. (2011) Defense and counterdefense in the RNAi-based antiviral immune system in insects. *Methods Mol. Biol.*, **721**, 3–22.
4. Chung,W.J., Okamura,K., Martin,R. and Lai,E.C. (2008) Endogenous RNA interference provides a somatic defense against Drosophila transposons. *Curr. Biol.*, **18**, 795–802.
5. Czech,B., Malone,C.D., Zhou,R., Stark,A., Schlingeheyde,C., Dus,M., Perrimon,N., Kellis,M., Wohlschlegel,J.A., Sachidanandam,R. *et al.* (2008) An endogenous small interfering RNA pathway in Drosophila. *Nature*, **453**, 798–802.
6. Ghildiyal,M., Seitz,H., Horwich,M.D., Li,C., Du,T., Lee,S., Xu,J., Kittler,E.L., Zapp,M.L., Weng,Z. *et al.* (2008) Endogenous siRNAs derived from transposons and mRNAs in Drosophila somatic cells. *Science*, **320**, 1077–1081.
7. Okamura,K., Chung,W.J., Ruby,J.G., Guo,H., Bartel,D.P. and Lai,E.C. (2008) The Drosophila hairpin RNA pathway generates endogenous short interfering RNAs. *Nature*, **453**, 803–806.
8. Liu,Q., Rand,T.A., Kalidas,S., Du,F., Kim,H.E., Smith,D.P. and Wang,X. (2003) R2D2, a bridge between the initiation and effector steps of the Drosophila RNAi pathway. *Science*, **301**, 1921–1925.
9. Denli,A.M., Tops,B.B., Plasterk,R.H., Ketting,R.F. and Hannon,G.J. (2004) Processing of primary microRNAs by the Microprocessor complex. *Nature*, **432**, 231–235.
10. Han,J., Lee,Y., Yeom,K.H., Kim,Y.K., Jin,H. and Kim,V.N. (2004) The Drosha-DGCR8 complex in primary microRNA processing. *Genes Dev.*, **18**, 3016–3027.
11. Landthaler,M., Yalcin,A. and Tuschl,T. (2004) The human DiGeorge syndrome critical region gene 8 and Its D. melanogaster homolog are required for miRNA biogenesis. *Curr. Biol.: CB*, **14**, 2162–2167.
12. Chendrimada,T.P., Gregory,R.I., Kumaraswamy,E., Norman,J., Cooch,N., Nishikura,K. and Shiekhattar,R. (2005) TRBP recruits the Dicer complex to Ago2 for microRNA processing and gene silencing. *Nature*, **436**, 740–744.
13. Forstemann,K., Tomari,Y., Du,T., Vagin,V.V., Denli,A.M., Bratu,D.P., Klattenhoff,C., Theurkauf,W.E. and Zamore,P.D. (2005) Normal microRNA maturation and germ-line stem cell maintenance requires Loquacious, a double-stranded RNA-binding domain protein. *PLoS Biol.*, **3**, e236.
14. Jiang,F., Ye,X., Liu,X., Fincher,L., McKearin,D. and Liu,Q. (2005) Dicer-1 and R3D1-L catalyze microRNA maturation in Drosophila. *Genes Dev.*, **19**, 1674–1679.
15. Bycroft,M., Grunert,S., Murzin,A.G., Proctor,M. and St Johnston,D. (1995) NMR solution structure of a dsRNA binding domain from Drosophila staufen protein reveals homology to the N-terminal domain of ribosomal protein S5. *EMBO J.*, **14**, 3563–3571.
16. Kharrat,A., Macias,M.J., Gibson,T.J., Nilges,M. and Pastore,A. (1995) Structure of the dsRNA binding domain of E. coli RNase III. *EMBO J.*, **14**, 3572–3584.
17. Doyle,M. and Jantsch,M.F. (2002) New and old roles of the double-stranded RNA-binding domain. *J. Struct. Biol.*, **140**, 147–153.
18. Yamashita,S., Nagata,T., Kawazoe,M., Takemoto,C., Kigawa,T., Guntert,P., Kobayashi,N., Terada,T., Shirouzu,M., Wakiyama,M. *et al.* (2011) Structures of the first and second double-stranded RNA-binding domains of human TAR RNA-binding protein. *Protein Sci.*, **20**, 118–130.
19. Ryter,J.M. and Schultz,S.C. (1998) Molecular basis of double-stranded RNA-protein interactions: structure of a dsRNA-binding domain complexed with dsRNA. *EMBO J.*, **17**, 7505–7513.
20. Huang,Y., Ji,L., Huang,Q., Vassylyev,D.G., Chen,X. and Ma,J.B. (2009) Structural insights into mechanisms of the small RNA methyltransferase HEN1. *Nature*, **461**, 823–827.
21. Stefl,R., Oberstrass,F.C., Hood,J.L., Jourdan,M., Zimmermann,M., Skrisovska,L., Maris,C., Peng,L., Hofr,C., Emeson,R.B. *et al.* (2010) The solution structure of the ADAR2 dsRBM-RNA complex reveals a sequence-specific readout of the minor groove. *Cell*, **143**, 225–237.
22. Nanduri,S., Carpick,B.W., Yang,Y., Williams,B.R. and Qin,J. (1998) Structure of the double-stranded RNA-binding domain of the protein kinase PKR reveals the molecular basis of its dsRNA-mediated activation. *EMBO J.*, **17**, 5458–5465.
23. Sohn,S.Y., Bae,W.J., Kim,J.J., Yeom,K.H., Kim,V.N. and Cho,Y. (2007) Crystal structure of human DGCR8 core. *Nat. Struct. Mol. Biol.*, **14**, 847–853.
24. Jayachandran,U., Grey,H. and Cook,A.G. (2016) Nuclear factor 90 uses an ADAR2-like binding mode to recognize specific bases in dsRNA. *Nucleic Acids Res.*, **44**, 1924–1936.
25. Tian,B. and Mathews,M.B. (2001) Functional characterization of and cooperation between the double-stranded RNA-binding motifs of the protein kinase PKR. *J. Biol. Chem.*, **276**, 9936–9944.
26. Wang,X., Vukovic,L., Koh,H.R., Schulten,K. and Myong,S. (2015) Dynamic profiling of double-stranded RNA binding proteins. *Nucleic Acids Res.*, **43**, 7566–7576.
27. Khvorova,A., Reynolds,A. and Jayasena,S.D. (2003) Functional siRNAs and miRNAs exhibit strand bias. *Cell*, **115**, 209–216.
28. Schwarz,D.S., Hutvagner,G., Du,T., Xu,Z., Aronin,N. and Zamore,P.D. (2003) Asymmetry in the assembly of the RNAi enzyme complex. *Cell*, **115**, 199–208.
29. Mi,S., Cai,T., Hu,Y., Chen,Y., Hodges,E., Ni,F., Wu,L., Li,S., Zhou,H., Long,C. *et al.* (2008) Sorting of small RNAs into Arabidopsis argonaute complexes is directed by the 5' terminal nucleotide. *Cell*, **133**, 116–127.
30. Takeda,A., Iwasaki,S., Watanabe,T., Utsumi,M. and Watanabe,Y. (2008) The mechanism selecting the guide strand from small RNA duplexes is different among argonaute proteins. *Plant Cell Physiol.*, **49**, 493–500.
31. Montgomery,T.A., Howell,M.D., Cuperus,J.T., Li,D., Hansen,J.E., Alexander,A.L., Chapman,E.J., Fahlgren,N., Allen,E. and Carrington,J.C. (2008) Specificity of ARGONAUTE7-miR390 interaction and dual functionality in TAS3 trans-acting siRNA formation. *Cell*, **133**, 128–141.
32. Tomari,Y., Matranga,C., Haley,B., Martinez,N. and Zamore,P.D. (2004) A protein sensor for siRNA asymmetry. *Science*, **306**, 1377–1380.
33. Noland,C.L., Ma,E. and Doudna,J.A. (2011) siRNA repositioning for guide strand selection by human Dicer complexes. *Mol. Cell*, **43**, 110–121.
34. Noland,C.L. and Doudna,J.A. (2013) Multiple sensors ensure guide strand selection in human RNAi pathways. *RNA*, **19**, 639–648.
35. Pham,J.W., Pellino,J.L., Lee,Y.S., Carthew,R.W. and Sontheimer,E.J. (2004) A Dicer-2-dependent 80s complex cleaves targeted mRNAs during RNAi in Drosophila. *Cell*, **117**, 83–94.
36. Gredell,J.A., Dittmer,M.J., Wu,M., Chan,C. and Walton,S.P. (2010) Recognition of siRNA asymmetry by TAR RNA binding protein. *Biochemistry*, **49**, 3148–3155.
37. Liang,C., Wang,Y., Murota,Y., Liu,X., Smith,D., Siomi,M.C. and Liu,Q. (2015) TAF11 Assembles the RISC Loading Complex to Enhance RNAi Efficiency. *Mol. Cell*, **59**, 807–818.
38. Kim,Y., Yeo,J., Lee,J.H., Cho,J., Seo,D., Kim,J.S. and Kim,V.N. (2014) Deletion of human tarbp2 reveals cellular microRNA targets and cell-cycle function of TRBP. *Cell Rep.*, **9**, 1061–1074.
39. Betancur,J.G. and Tomari,Y. (2012) Dicer is dispensable for asymmetric RISC loading in mammals. *RNA*, **18**, 24–30.
40. Marques,J.T., Kim,K., Wu,P.H., Alleyne,T.M., Jafari,N. and Carthew,R.W. (2010) Loqs and R2D2 act sequentially in the siRNA pathway in Drosophila. *Nat. Struct. Mol. Biol.*, **17**, 24–30.
41. Nishida,K.M., Miyoshi,K., Ogino,A., Miyoshi,T., Siomi,H. and Siomi,M.C. (2013) Roles of R2D2, a cytoplasmic D2 body component, in the endogenous siRNA pathway in Drosophila. *Mol. Cell*, **49**, 680–691.
42. Mirkovic-Hosle,M. and Forstemann,K. (2014) Transposon defense by endo-siRNAs, piRNAs and somatic pilRNAs in Drosophila: contributions of Loqs-PD and R2D2. *PLoS One*, **9**, e84994.
43. Delaglio,F., Grzesiek,S., Vuister,G.W., Zhu,G., Pfeifer,J. and Bax,A. (1995) NMRPipe: a multidimensional spectral processing system based on UNIX pipes. *J. Biomol. NMR*, **6**, 277–293.
44. Sattler,M., Schleucher,J. and Griesinger,C. (1999) Heteronuclear multidimensional NMR experiments for the structure determination of proteins in solution employing pulsed field gradients. *J. Biomol. NMR*, **6**, 277–293.
45. Shah,C. and Forstemann,K. (2008) Monitoring miRNA-mediated silencing in Drosophila melanogaster S2-cells. *Biochim. Biophys. Acta*, **1779**, 766–772.
46. Schmidts,I., Bottcher,R., Mirkovic-Hosle,M. and Forstemann,K. (2016) Homology directed repair is unaffected by the absence of

siRNAs in Drosophila melanogaster. *Nucleic Acids Res.*, **44**, 8261–8271.
47. Hartig,J.V., Esslinger,S., Bottcher,R., Saito,K. and Forstemann,K. (2009) Endo-siRNAs depend on a new isoform of loquacious and target artificially introduced, high-copy sequences. *EMBO J.*, **28**, 2932–2944.
48. Miyoshi,K., Miyoshi,T., Hartig,J.V., Siomi,H. and Siomi,M.C. (2010) Molecular mechanisms that funnel RNA precursors into endogenous small-interfering RNA and microRNA biogenesis pathways in Drosophila. *RNA*, **16**, 506–515.
49. Zhou,R., Czech,B., Brennecke,J., Sachidanandam,R., Wohlschlegel,J.A., Perrimon,N. and Hannon,G.J. (2009) Processing of Drosophila endo-siRNAs depends on a specific Loquacious isoform. *RNA*, **15**, 1886–1895.
50. Cenik,E.S., Fukunaga,R., Lu,G., Dutcher,R., Wang,Y., Tanaka Hall,T.M. and Zamore,P.D. (2011) Phosphate and R2D2 restrict the substrate specificity of Dicer-2, an ATP-driven ribonuclease. *Mol. Cell*, **42**, 172–184.
51. Okamura,K., Robine,N., Liu,Y., Liu,Q. and Lai,E.C. (2010) R2D2 organizes small regulatory RNA pathways in Drosophila. *Mol. Cell. Biol.*, **31**, 884–896.
52. Hartig,J.V. and Forstemann,K. (2011) Loqs-PD and R2D2 define independent pathways for RISC generation in Drosophila. *Nucleic Acids Res.*, **39**, 3836–3851.
53. Zhou,R., Hotta,I., Denli,A.M., Hong,P., Perrimon,N. and Hannon,G.J. (2008) Comparative analysis of argonaute-dependent small RNA pathways in Drosophila. *Mol. Cell*, **32**, 592–599.
54. Vagin,V.V., Sigova,A., Li,C., Seitz,H., Gvozdev,V. and Zamore,P.D. (2006) A distinct small RNA pathway silences selfish genetic elements in the germline. *Science*, **313**, 320–324.
55. Elmer,K., Helfer,S., Mirkovic-Hosle,M. and Forstemann,K. (2014) Analysis of endo-siRNAs in Drosophila. *Methods Mol. Biol.*, **1173**, 33–49.
56. Shamoo,Y., Abdul-Manan,N. and Williams,K.R. (1995) Multiple RNA binding domains (RBDs) just don't add up. *Nucleic Acids Res.*, **23**, 725–728.
57. Neumuller,R.A., Richter,C., Fischer,A., Novatchkova,M., Neumuller,K.G. and Knoblich,J.A. (2011) Genome-wide analysis of self-renewal in Drosophila neural stem cells by transgenic RNAi. *Cell Stem Cell*, **8**, 580–593.
58. Wunderlich,C.H., Huber,R.G., Spitzer,R., Liedl,K.R., Kloiber,K. and Kreutz,C. (2013) A novel paramagnetic relaxation enhancement tag for nucleic acids: a tool to study structure and dynamics of RNA. *ACS Chem. Biol.*, **8**, 2697–2706.
59. Wunderlich,C.H., Juen,M.A., LeBlanc,R.M., Longhini,A.P., Dayie,T.K. and Kreutz,C. (2015) Stable isotope-labeled RNA phosphoramidites to facilitate dynamics by NMR. *Methods Enzymol.*, **565**, 461–494.
60. Gobl,C., Madl,T., Simon,B. and Sattler,M. (2014) NMR approaches for structural analysis of multidomain proteins and complexes in solution. *Prog. Nucl. Magn. Reson. Spectrosc.*, **80**, 26–63.
61. Clore,G.M. and Iwahara,J. (2009) Theory, practice, and applications of paramagnetic relaxation enhancement for the characterization of transient low-population states of biological macromolecules and their complexes. *Chem. Rev.*, **109**, 4108–4139.
62. Bottcher,R., Hollmann,M., Merk,K., Nitschko,V., Obermaier,C., Philippou-Massier,J., Wieland,I., Gaul,U. and Forstemann,K. (2014) Efficient chromosomal gene modification with CRISPR/cas9 and PCR-based homologous recombination donors in cultured Drosophila cells. *Nucleic Acids Res.*, **42**, e89.
63. Wang,Y.M., Tegenfeldt,J.O., Reisner,W., Riehn,R., Guan,X.J., Guo,L., Golding,I., Cox,E.C., Sturm,J. and Austin,R.H. (2005) Single-molecule studies of repressor-DNA interactions show long-range interactions. *Proc. Natl. Acad. Sci. U.S.A.*, **102**, 9796–9801.
64. Kim,S., Brostromer,E., Xing,D., Jin,J., Chong,S., Ge,H., Wang,S., Gu,C., Yang,L., Gao,Y.Q. *et al.* (2013) Probing allostery through DNA. *Science*, **339**, 816–819.
65. Tomari,Y., Du,T., Haley,B., Schwarz,D.S., Bennett,R., Cook,H.A., Koppetsch,B.S., Theurkauf,W.E. and Zamore,P.D. (2004) RISC assembly defects in the Drosophila RNAi mutant armitage. *Cell*, **116**, 831–841.
66. Merk,K., Breinig,M., Bottcher,R., Krebs,S., Blum,H., Boutros,M. and Forstemann,K. (2017) Splicing stimulates siRNA formation at Drosophila DNA double-strand breaks. *PLoS Genet.*, **13**, e1006861.
67. Rohrl,C., Meisslitzer-Ruppitsch,C., Bittman,R., Li,Z., Pabst,G., Prassl,R., Strobl,W., Neumuller,J., Ellinger,A., Pavelka,M. *et al.* (2012) Combined light and electron microscopy using diaminobenzidine photooxidation to monitor trafficking of lipids derived from lipoprotein particles. *Curr. Pharm. Biotechnol.*, **13**, 331–340.
68. Leitinger,G., Masich,S., Neumuller,J., Pabst,M.A., Pavelka,M., Rind,F.C., Shupliakov,O., Simmons,P.J. and Kolb,D. (2012) Structural organization of the presynaptic density at identified synapses in the locust central nervous system. *J. Comp. Neurol.*, **520**, 384–400.
69. Esslinger,S.M., Schwalb,B., Helfer,S., Michalik,K.M., Witte,H., Maier,K.C., Martin,D., Michalke,B., Tresch,A., Cramer,P. *et al.* (2013) Drosophila miR-277 controls branched-chain amino acid catabolism and affects lifespan. *RNA Biol.*, **10**, 1042–1056.
70. Giuliani,F., Giuliani,G., Bauer,R. and Rabouille,C. (2013) Innexin 3, a new gene required for dorsal closure in Drosophila embryo. *PLoS One*, **8**, e69212.
71. Giuliani,G., Giuliani,F., Volk,T. and Rabouille,C. (2014) The Drosophila RNA-binding protein HOW controls the stability of dgrasp mRNA in the follicular epithelium. *Nucleic Acids Res.*, **42**, 1970–1986.
72. Glisovic,T., Bachorik,J.L., Yong,J. and Dreyfuss,G. (2008) RNA-binding proteins and post-transcriptional gene regulation. *FEBS Lett.*, **582**, 1977–1986.
73. Koh,H.R., Kidwell,M.A., Ragunathan,K., Doudna,J.A. and Myong,S. (2013) ATP-independent diffusion of double-stranded RNA binding proteins. *Proc. Natl. Acad. Sci. U.S.A.*, **110**, 151–156.
74. Murchison,E.P., Partridge,J.F., Tam,O.H., Cheloufi,S. and Hannon,G.J. (2005) Characterization of Dicer-deficient murine embryonic stem cells. *Proc. Natl. Acad. Sci. U.S.A.*, **102**, 12135–12140.
75. Kawamata,T. and Tomari,Y. (2010) Making RISC. *Trends Biochem. Sci.*, **35**, 368–376.
76. Sinha,N.K., Trettin,K.D., Aruscavage,P.J. and Bass,B.L. (2015) Drosophila dicer-2 cleavage is mediated by helicase- and dsRNA termini-dependent states that are modulated by Loquacious-PD. *Mol. Cell*, **58**, 406–417.
77. Markstein,M., Dettorre,S., Cho,J., Neumuller,R.A., Craig-Muller,S. and Perrimon,N. (2014) Systematic screen of chemotherapeutics in Drosophila stem cell tumors. *Proc. Natl. Acad. Sci. U.S.A.*, **111**, 4530–4535.
78. Yan,D., Neumuller,R.A., Buckner,M., Ayers,K., Li,H., Hu,Y., Yang-Zhou,D., Pan,L., Wang,X., Kelley,C. *et al.* (2014) A regulatory network of Drosophila germline stem cell self-renewal. *Dev. Cell*, **28**, 459–473.